J Electroceram (2011) 27:169–175
DOI 10.1007/s10832-011-9662-7

Leakage current analysis of hydrothermal $BaTiO_3$ thin films

P. Markondeya Raj · Baik-Woo Lee ·
Devarajan Balaraman · Rao R. Tummala

Received: 10 January 2011 / Accepted: 28 October 2011 / Published online: 19 November 2011
© Springer Science+Business Media, LLC 2011

Abstract Hydrothermal processing can deposit crystalline ferroelectric films at low temperatures of less than 150°C to achieve permittivities above 100. Such a process, hence, can be attractive in integrating thin film capacitors in organic, silicon or flex substrates. However, their poor insulation strength leading to high leakage current can prevent their wide acceptance. Lattice defects such as hydroxyl groups are attributed to their high leakage currents and lower Breakdown Voltages (BDVs). With appropriate thermal treatments, majority of the OH groups can be removed, leading to improved insulation characteristics. The leakage current behavior of as-synthesized and post-baked hydrothermal thin films are analyzed with various conduction models. The room temperature I-V characteristics are attributed to a combination of ionic and Space-Charge-Limited (SCLC) conduction models for films baked at 160°C while higher baking temperatures of 350°C agree well with Poole-Frenkel type conduction, with an activation energy of 0.57 eV for the defects. The defects, which are presumably OH groups or oxygen vacancies embedded in the barium titanate lattice, act as shallow traps and the trapping and detrapping results in easier conduction. A brief perspective is provided on the suitability of such a hydrothermal thin film capacitor approach for power supply applications.

Keywords Barium titanate · Hydrothermal films · Leakage currents · Decoupling capacitors · Embedded passives · Poole-Frenkel conduction · Ionic conduction

P. M. Raj (✉) · B.-W. Lee · D. Balaraman · R. R. Tummala
3D Systems Packaging Research Center,
Georgia Institute of Technology,
Atlanta, GA 30332, USA
e-mail: raj@ece.gatech.edu

1 Introduction

Low-temperature synthesis enables integration of high permittivity thin films in electronic packages. Such an approach can have a tremendous impact in miniaturization of packages, by replacing bulky surface-mounted capacitors [1, 2]. Research in high permittivity (K) thin film capacitors on silicon has been primarily motivated by memory and processor ICs for storage cells and gate dielectrics in the past. Recently, decoupling capacitor application has been the primary driver for integrating high K thin films. These capacitors supply current in milli to nanosecond time intervals to allow various processor operations, thus minimizing excessive voltage fluctuations to provide noise-free power supply in high-speed digital circuits. The current transients are of nanosecond intervals during logic operations within the microprocessor, medium duration of microseconds when the microprocessor communicates with memory through package, and longer-duration of milliseconds when the processor communicates with the hard-drive on the printed wiring board (PWB). The Voltage Regulator Modules (VRMs) typically respond in millisecond intervals. Therefore, decoupling capacitors are used at mid- and high frequencies to supply the current transients and enable noise-free power supply.

Thin film decoupling in the package offers several advantages over the traditional discrete surface-mount capacitors. Embedded thin film capacitors have much lower inductance and hence expand the operating frequency. They also save valuable real estate, whether they are on chip, package or board because they are typically in micron dimensions compared to millimeter dimensions of discrete passives. Elimination of assembly cost and solder joint reliability concerns are other advantages of embedding decoupling capacitors. A distributed-set of decoupling

capacitors, however, is required to address the current transient needs at various levels of systems from IC to package to system board. Hence, novel decoupling schemes are being continuously developed to address the power integrity issues in high-speed digital systems. Three technologies have recently received wide attention for thin film embedded decoupling capacitors: 1. Polymer-ceramic composites, 2. Silicon-compatible inorganic thin film capacitors, and 3. Solgel processed capacitors on copper foil and subsequent foil lamination in organic packages. All these thin film decoupling capacitor technologies have been widely reviewed recently [1–3].

Polymer composites typically do not achieve more than 50 nF/cm^2 because of their lower permittivity at composite level and thicker films, although they are compatible with organic package fabrication [3]. Reliable and manufacturable composite films have capacitance densities of less than 20 nF/cm^2. Integration of higher permittivity inorganic thin films in organic packages leads to several process-incompatibilities and manufacturability issues that arise when processing these films at high temperatures to crystallize them. One way to solve this thermal incompatibility problem is by processing the high K films on bare, free-standing copper foils and subsequently laminating the foil onto the organic package. However, such a process creates several manufacturing challenges [4, 5]. The other way to address the need is by integration within CMOS or its back-end compatible thin film capacitors. Such capacitor dielectrics are usually relegated to moderate permittivity such as by silicon dioxide or tantalum oxide with capacitance densities of 20–200 nF/cm^2. Further enhancement in capacitance densities requires silicon trench structures for higher surface area.

Hydrothermal nanocrystalline $BaTiO_3$ is of major interest for decoupling applications because it can be synthesized as thinner films with higher yield and higher capacitance density of 1000 nF/cm^2 at lower temperatures, leading to thin film components that can potentially be integrated in organic or silicon substrates.

Hydrothermal thin film crystallization involves nucleation and growth of $BaTiO_3$ or other grains on a substrate by reacting metallic titanium [6] or titanium precursor coatings [7] with barium ions in an alkaline medium at 80–150°C. The deposited ceramic films are compatible with subsequent processing at higher temperatures. Because of its reactive and self-limiting nature, it leads to conformality and uniformity in dielectric thickness over the entire substrate. Hydrothermal crystallization can be explained through two different mechanisms, in-situ transformation and dissolution-precipitation, both of which are based on the general nucleation-growth phenomena. With in-situ transformation, barium reacts, at the surface of the hydrated titania, to form an inwardly growing film of crystalline barium titanate. In the dissolution-precipitation mechanism, titania dissolves and heterogeneous nucleation of barium titanate occurs at the film-solution interface. Eckert et al. [8] observe that the dissolution-precipitation process occurs at the beginning while the in-situ transformation mechanism evolves over longer reaction times.

In hydrothermal $BaTiO_3$ synthesis, water and hydroxyl groups (OH^-) can be easily incorporated into the crystal because all reactions are carried out under an aqueous, highly- alkaline environment. The OH groups exist both on the surface and in the lattice while water is proposed to exist in a highly defective shell that forms on the outside of the hydrothermal grains [9]. Oxygen vacancies and carbonate ion impurities are also incorporated into the lattice. Dielectric properties of hydrothermal $BaTiO_3$ are sensitive to the hydroxyl groups. McCormick and Slamovich [10] observed gradual decrease in the dielectric constants, dielectric losses and leakage current with decreasing concentration of hydroxyl groups in hydrothermal $BaTiO_3$ films through heat treatments ranging from 200°C to 500°C. Chien et al. [11] also reported the dependence of dielectric properties on hydroxyl groups in baked hydrothermal, hetero-epitaxial thin films. In their hydrothermal films, baking at 200°C initially resulted in a significant decrease in dielectric constant but an increase in dielectric loss followed by a recovery of dielectric constants and a marked decrease in dielectric losses at 400–600°C. Kota and Lee also observed and proposed an inverse relationship between hydroxyl groups and dielectric properties [12].

Though several studies are reported on the chemical and structural characteristics of hydrothermal films, very few studies focused on the electrical properties beyond the capacitance density studies. Analysis of leakage currents and the conduction mechanisms can provide important information on the nature of defects in hydrothermal films, defect concentration and the activation energy. Systematic correlation of these parameters to the material chemistry and process conditions can provide fundamental guidelines towards suppressing leakage currents in hydrothermal thin films. The objectives of this research are therefore to analyze and model leakage currents in as-synthesized and baked hydrothermal films to understand the conduction mechanisms.

2 Experimental methods

Hydrothermal synthesis of $BaTiO_3$ films involves bringing together suitable titanium and barium sources in an alkaline solution. In this study, Ti/Cu/Ti was first evaporated on Si-wafers. The bottom 20 nm Ti acts as an adhesion layer. The 100 nm top Ti layer was used as the titanium source for the hydrothermal $BaTiO_3$ synthesis. Hydrothermal bath was prepared by dissolving barium hydroxide (Reagent grade)

in boiling deionized water. Boiling helps to reduce the dissolved carbon dioxide in the water that can form insoluble carbonates. Further, the solution was prepared in a glove box purged with nitrogen to minimize contact with carbon-dioxide. Despite these precautions, precipitates were invariably found in the solution due to carbonates present as impurities in the reagent grade barium hydroxide. Such precipitates were minimized by allowing them to settle in tall polypropylene bottles for at least 6 h. The clear solution on the top was then filtered through a 30 μm nylon mesh into polystyrene reaction containers in the glove box. The pH of the solution was measured to be 13.5 at 95°C. The optimum $Ba(OH)_2$ concentration for hydrothermal $BaTiO_3$ synthesis was found to be 2 M from the authors' earlier studies [13]. The Ti-film on Si-wafer was placed facing down on Teflon frames in the solution in order to avoid precipitates from settling onto the surface and locally inhibiting formation of $BaTiO_3$. The reaction was allowed to proceed for 24 h in an oven at 95°C. Hydrothermal synthesis temperatures were chosen to be below 100°C to avoid the use of autoclaves. The samples were then removed from the reaction container and rinsed in deionized water and baked at 160°C in a convection oven for 15 min. For reducing the concentration of hydroxyl groups, the initially synthesized $BaTiO_3$ films were baked at 350°C. The annealing temperatures were limited to 350°C so that the film grain structure and $BaTiO_3$/Ti interfaces are stable.

Morphology of the film cross-sections was studied with Scanning Electron Microscopy (LEO 1530 Thermally-Assisted Field Emission SEM). Composition analysis as a function of depth was performed with X-Ray Photo-electron Spectroscopy (Thermo-Fisher, K-Alpha XPS). Argon ion-etching with 1000 eV was used to etch the film and obtain the composition of Ba, Ti, O and C as a function of depth. Each etch-step consists of ion-etching for 13 s. Since the exact etch rates are not known and vary with composition and baking, the number of etch cycles is only a qualitative index of the depth at which the composition is obtained.

Dielectric measurements were carried out using parallel plate capacitor structures. The un-reacted titanium coupled with the underlying copper served as bottom electrode while the top electrode was 500 nm thick gold evaporated through a shadow mask. Capacitances and loss tangents were measured by employing HP 4285A LCR meter (Agilent Technologies Inc., Englewood, CO) at 100 kHz. DC leakage measurements were performed using a semiconductor parameter analyzer (Hewlett Packard Model 4155). The voltage and current limits of the instrument were 20 V and 100 mA, respectively. The voltage was increased in steps of 50 mV till the current reached the 100 mA due to permanent breakdown or otherwise. The current was measured with 1 s delay.

3 Results and discussion

The detailed material characterization of hydrothermal barium titanate thin films was discussed in an earlier publication [14] and are not shown here. The films show dense barium titanate grains with an average size of 80 nm. A cross-section of the as-synthesized film is shown in Fig. 1. The films consist of a single layer of barium titanate grains. SEM cross-sections show a thickness of 90 nm for the top ceramic film. The grains are much larger than those obtained from solgel and CVD processing for similar thicknesses. This is because of the faster crystal nucleation and growth in the alkaline medium compared to the solid state nucleation and growth that happens in solgel process. The film consists of dense barium titanate films with minimal porosity. However, the film is not stoichiometrically pure because of embedded OH groups, residual carbonates on the surface and a diffuse titania-rich interface as seen from X-ray Photo-electron Spectroscopy (Fig. 2). XPS results are discussed later in detail.

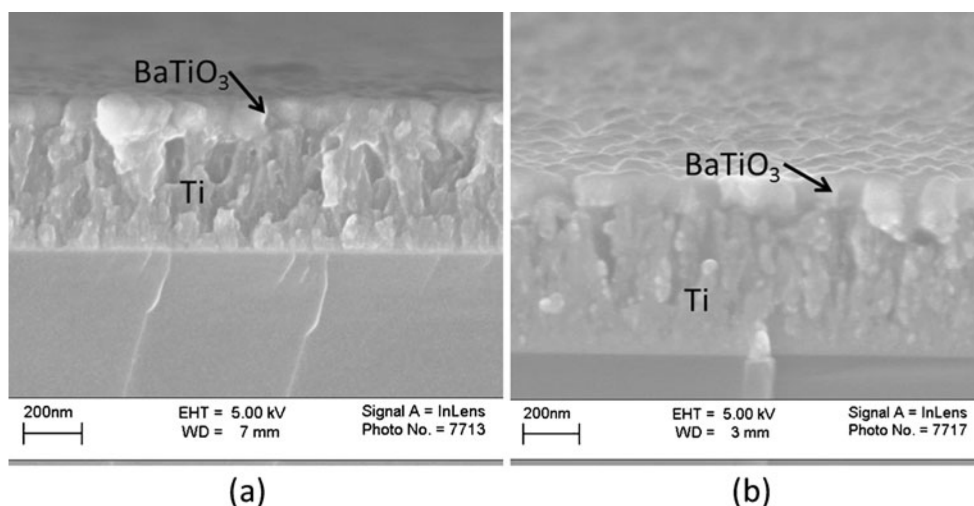

Fig. 1 SEM cross-section of the hydrothermal barium titanate film on an evaporated titanium film – (**a**) 160°C baking, (**b**) 350°C baking

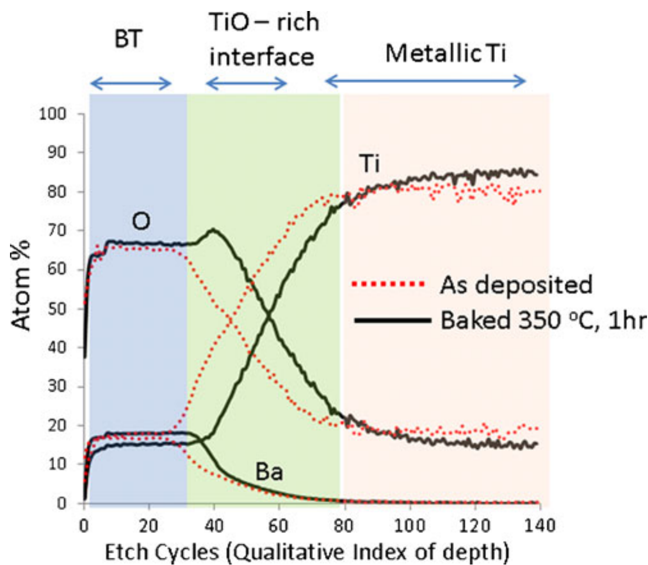

Fig. 2 XPS composition analysis as a function of etching time

The bottom part of the film is from the evaporated titanium while dense and pin-hole free barium titanate grains are seen on the top. XRD and Raman Spectroscopy studies show crystalline barium titanate structure as published in the earlier report [14]. Typical capacitance densities and dielectric losses of the hydrothermal $BaTiO_3$ films are shown in Table 1. The dielectric constants are estimated from the thickness measurements by SEM of the film cross-sections. The capacitance density and dielectric loss for as-synthesized film measured at 100 kHz are ~2 $\mu F/cm^2$ and 0.3, respectively. The dielectric loss was much higher than 0.02 seen in typical $BaTiO_3$ bulk films. Baking at higher temperatures induced significant reduction in the capacitances and dielectric losses. When baked at package-compatible temperatures of 160°C, the films showed a dielectric constant of 119 and loss tangent of 0.075. Their very low dielectric constant, compared to 6000 ~7000 of submicron-grained $BaTiO_3$, indicates that the film lost its ferroelectricity to a large extent. This phenomenon is well-reported and understood in nano-grained $BaTiO_3$. Further, the low permittivity suggests the presence of an amorphous titania layer under the crystalline barium titanate. These dielectric characteristics are very consistent with McCormick and Slamovich's results, showing an initial decrease in the dielectric constants and losses with increasing baking temperatures of hydrothermal $BaTiO_3$ films [10]. Further heat treatment at higher temperature is expected to recover the dielectric constant. However, baking at temperatures above 350°C reduces the effective dielectric constant in this case because of the thickened titania layer underneath the barium titanate film [14].

SEM cross-sections did not show any difference before and after baking at 350°C as shown in Fig. 1b. XPS was used as the complementary technique to obtain the differences in film composition before and after baking, as shown in Fig. 2. The first two etch-steps show surface contamination from oxygen and carbon, while the next 3–4 layers show carbon from surface barium carbonate. The next 20–30 cycles show $BaTiO_3$, followed by a TiO-rich interface for 40–50 cycles and metallic titanium. The metallic titanium showed 20% oxygen because of the non-ideal e-beam evaporation conditions used during the film deposition or the oxygen contamination of the e-beam crucible. The interface between $BaTiO_3$ and Ti is not sharp and has gradual change in the concentration from the ceramic to the metal. The diffuse interface predominantly consists of non-stoichiometric Ti-O which gets thicker with higher baking temperatures as seen from XPS. Based on the XPS composition profile, approximately 30% increase in thickness is attributed to the baked film, corresponding to 120 nm thickness. The leakage current of the baked films was modeled using this thickness.

Baking the films had a strong effect on the leakage current characteristics of the films. Fig. 3 shows the current-voltage (I-V) characteristics for as-synthesized and baked $BaTiO_3$ films. The breakdown voltages for the films baked at 350°C were improved to 20 V, compared to as-synthesized film with 2–5 V. The leakage current density of 350°C-baked film is more than five orders of magnitude lower than that of the as-synthesized film at 2 V.

The leakage current characteristics were fit to various models in order to allude to the conduction mechanisms. The conduction mechanisms that are frequently reported in thin ceramic films are ionic, Schottky, Poole-Frenkel and Space-Charge-Limited Conduction (SCLC) and are summarized in Table 2. For films baked at 160 ºC, the I-V fits were not consistent with Poole-Frenkel or Schottky models because the extracted dynamic permittivities from the slopes of $\ln(J)$-$E^{1/2}$ and $\ln(J/E)$-$E^{1/2}$ were found to be less than 1. The log-log I-V fit with SCLC model shows a slope

Table 1 Dielectric properties of hydrothermal $BaTiO_3$ films in this study

Thermal treatment	Capacitance density $\mu F/cm^2$	Thickness	Dielectric constant	Dielectric loss
As-deposited	2	90 nm	203	0.3
160°C	1.17	90 nm	119	0.075
350°C	0.79	120 nm	107	0.040

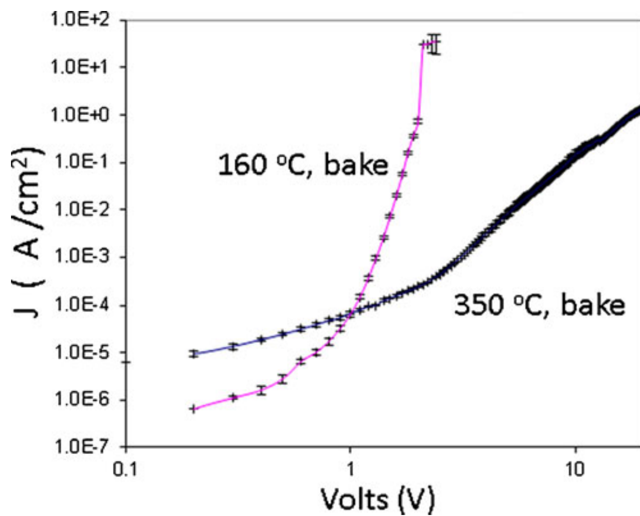

Fig. 3 Log(J) Vs Log(V) curves obtained from the hydrothermal $BaTiO_3$ films baked at 350 C compared to films baked at 160°C

of ~16 at high electric fields, which is not consistent with the theoretical value of 2 for a trap-free SCLC and far above than the usually observed values in literature. However, an insulator in which the traps are distributed uniformly in energy levels below the conduction band can give raise to SCLC slopes much above 2 [15]. Hence, SCLC can be attributed as a dominant mechanism for the leakage current. The hydrothermal films with low work-function titanium underneath have lower barrier height for easy thermionic emission. In combination with the high density of defects that act as charge carriers within the film, this phenomenon usually leads to SCLC conduction.

For as-synthesized films, the I-V linearization also fits well to ionic conduction model giving the highest regression coefficient of 0.999. To verify this behavior, the leakage current was measured as a function of time at a fixed voltage and found to continuously increase. Current variation with time is usually attributed to the drift of lattice defects causing ionic conduction. Ionic conduction is accompanied by accumulation of defects or discharge of the ions as they arrive at the electrode interfaces because metal electrodes will block any mobile ionic defects. Measurements on as-synthesized films, therefore, indicate some contribution from ion migration-assisted leakage. The oxygen vacancies or protons incorporated with the hydroxyl groups are known to be effective charge carriers in such oxides.

The ionic current (J_{ion}) is expressed as:

$$J_{ion} = 2\lambda\nu e N \exp\left[\frac{-U}{kT}\right] \sinh\left[\frac{eE\lambda}{2kT}\right], \qquad (1)$$

where λ is the jump distance between potential wells, ν the attempt-to-escape frequency, e the electronic charge, N the ion density, U the activation energy, k Boltzmann constant and T the absolute temperature.

For high electric field (eEλ>kT), Eq. 1 can be approximated as:

$$J_{ion} = J_0(T) \quad e^{(\alpha E)}, \qquad (2)$$

where $J_0(T) = 2eN\lambda\nu \exp\left[\frac{-U}{kT}\right]$ and $\alpha = \frac{e\lambda}{2kT}$.

Substituting e = 1.6×10^{-19} Coulombs
k = 1.38×10^{-23} J/K
T = 298 K

The slope for ionic conduction can be simplified as:

$\alpha = 19.32\times10^{-9}\ \lambda$ where λ is in nm.

The slope of the ln(I) vs E for as-synthesized films baked at 160°C is 9×10^{-7} which estimates the jump distance λ as 46.5 nm. The jump distance is about 100 times higher than the lattice constant of barium titanate. Though similar jump

Table 2 Electronic conduction mechanisms examined in this work

Leakage current mechanism	Expression	Electric field dependence of leakage current
Space-Charge-Limited Conduction (SCLC)	$J = \frac{9\varepsilon_i\mu E^2}{8d^3}$ (ε_i: insulator dynamic permittivity, μ: carrier mobility, d: insulator thickness)	$J \sim E^2$
Schottky conduction	$J = A_1T^2\exp\left[\frac{-e(\phi_B-\sqrt{eE/4\pi\varepsilon_i})}{kT}\right]$ (A_1: the effective Richardson constant, e: electronic charge, ϕ_B: barrier height, ε_i: insulator dynamic permittivity, k: Boltzmann constant, T: Temperature)	$\ln(J) \sim E^{1/2}$
Poole-Frenkel conduction	$J = A_2E\exp\left(\frac{-e(\phi_B-\sqrt{eE/\pi\varepsilon_i})}{kT}\right)$ (A_2: constant, e: electronic charge, ϕ_B: barrier height, ε_i: insulator dynamic permittivity, k: Boltzmann constant, T: Temperature)	$\ln(J/E) \sim E^{1/2}$
Ionic conduction	$J_{ion} = J_0(T)\exp(\alpha E)$, where $J_0(T) = 2eN\lambda\nu\exp\left[\frac{-U}{kT}\right]$ and $\alpha = \frac{e\lambda}{2kT}$. λ is the jump distance between potential wells, ν is the attempt-to-escape frequency, e the electronic charge, N the ion density, U the activation energy, k Boltzmann constant and T the absolute temperature	In(J) ~ E

distances of 40 nm have been reported in the literature [16] in certain polymers, ionic conduction is not attributed to be the dominant conduction. A combination of SCLC and ionic conduction seems to be the main source for electronic conduction in films baked at 160°C. The leakage current analysis for films baked at 350°C is discussed below.

The FTIR (Fourier-Transform InfraRed) spectroscopy and TGA (Thermo Gravimetry Analysis) studies of baked films were consistent with previous observations that the out-gassing of absorbed water molecules occurs at temperatures below 200°C and elimination of lattice hydroxyl defects begins at 250°C [17]. Baking of hydrothermal films can leave an oxygen vacancy as shown by Chien et al. [12] as:

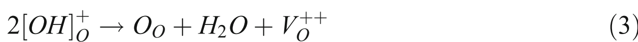

$$2[OH]_O^+ \rightarrow O_O + H_2O + V_O^{++} \tag{3}$$

Leakage current analysis of the I-V measurements from films that are baked at 350°C showed good fit (Fig. 4) and consistency with the Poole-Frenkel model compared to Schottky or SCLC indicating that Poole-Frenkel conduction is the dominant mechanism. For Poole-Frenkel conduction, the slope of ln(J/E)-$E^{1/2}$ is given as:

$$Slope = \frac{e^{1.5}}{kT\sqrt{\pi\varepsilon_o\varepsilon_r}} \equiv \frac{0.0028}{\sqrt{\varepsilon_r}} \tag{4}$$

after substituting

$\pi =$ 3.14;
$\varepsilon_0 =$ 8.854 x 10^{-12} F/m

The estimated optical dielectric constant from the slope is 7.84. This falls between the optical permittivity (~4.8) and the low frequency permittivity (~100). For Schottky fit, the estimated permittivity is 1.32 which is less than the optical permittivity of barium titanate and is hence considered to be inconsistent. The leakage current did not show strong polarity dependence though the electrode interfaces are strongly asymmetric in Ti/barium titanate/Au. Hence, the data suggests that the 350°C-baked films are mostly dominated by Poole-Frenkel mechanism while a combination of transport mechanisms dominated by ionic and SCLC conduction is suggested for the 160°C-baked films. As noted by McCormick and Slamovich, baking at 350°C effectively increases the barrier height by reducing the interfacial defect density [11] and suppresses the SCLC component of leakage current seen in films baked at 160°C. The activation energy for the defects was estimated from the I-T measurements at a voltage of 1.5 V. The leakage current measurements were performed at various temperatures while the device is heated. The voltage was applied at each temperature after the temperature was stabilized for 5 min. The leakage current behavior with temperature is linearized by plotting ln(J/E) vs 1/T and is shown in Fig. 5. From the slope of the linearized plot, the activation energy Φ can be estimated from the equation:

$$Slope = \frac{-e}{k}\left[\ \phi \ - \ \sqrt{\frac{eE}{\pi\,\varepsilon}}\ \right] \tag{5}$$

For 1.5 V across a 90 nm film with a relative permittivity of 7.8, substituting the slope of 5401 eV/K, Φ is estimated as 0.57 eV. The y intercepts from I-T can be used to estimate the Richardson constant (A). From the I-T equation:

$$\ln(A) \ = \ y \ \ intercept \ = \ -5.70 \tag{6}$$

The Richardson constant A is hence estimated to be 0.003 $(\text{ohm.cm})^{-1}$. The value of A is theoretically estimated as [18]:

$$A = eN_e\mu\alpha \tag{7}$$

where e is the electronic charge, N_e is the density of states, μ is the electronic mobility and α is equal to $(N_d\text{-}N_a)/N_a$. N_d

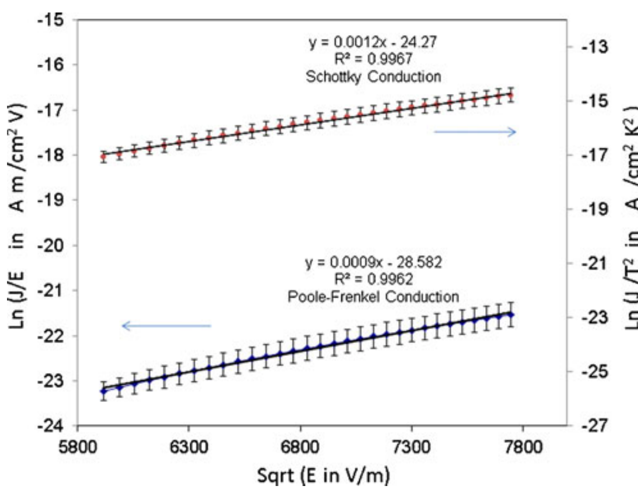

Fig. 4 Poole-Frenkel and Schottky fits for film baked at 350 C

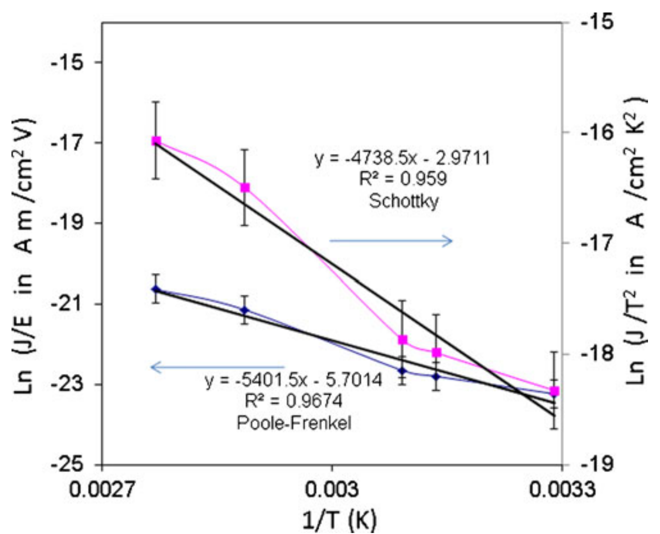

Fig. 5 Arrhenius fit for films baked at 350 C

and N_a represent the donor and acceptor concentrations. For a similar study on RF sputtered strontium titanate films that are 300 nm thick, Pennebaker estimated A as 6 $(ohm.cm)^{-1}$ and α equal to 0.003. Since μ and N_e are not known for hydrothermal barium titanate films, α cannot be accurately estimated.

The activation energy agrees with that reported in the literature [10, 19, 20] but are much lower that those seen in relatively defect-free barium titanate (3.95 eV [21]) indicating that the defects in baked hydrothermal films, which are presumably oxygen vacancies or lattice hydroxyls, act as shallow traps and the trapping and detrapping results in easier conduction.

Hydrothermal films show higher leakage currents and inferior capacitance densities, compared to films crystallized at high temperatures. This is the main limitation of hydrothermal films that has prevented its acceptance for commercial applications. Baking at temperatures of above 350°C can suppress the leakage current as shown here. Because of their highly reactive and conformal nature, these films can be deposited on high surface-area electrodes, which make them suitable to meet extremely high capacitance density targets. The benefits offered from low temperature processing that is compatible with organic package or silicon back-end process can make hydrothermal approach a viable technology option for several applications. Digital systems continuously move towards higher frequencies with higher data rates but with lower operating voltages. The BDV targets for these applications in future are expected to be lower, making hydrothermal approach more attractive for these applications. For some of these applications, the leakage current targets are not stringent because the encumbered power losses from the decoupling capacitors are a small fraction of the leakage power in the microprocessors. These capacitors can also be extended to as linear voltage regulators at low frequencies such as in DC-convertors.

On the other hand, many capacitor components such as in biomedical power supply applications operate at higher voltages to provide the neurostimulation functions. The leakage power directly affects the battery life in such applications, and hence lower leakage currents are required. Hence, significant improvements are needed in low temperature processed approaches such as by hydrothermal process described in this paper to meet these other set of applications.

4 Conclusionss

The properties of hydrothermal barium titanate films are strongly dependent on the embedded water groups in the perovskite lattice. The OH groups contribute to high leakage currents because of the ionic migration and SCLC. With thermal treatments, majority of the OH groups can be removed but the resultant defects still lead to inferior leakage currents. After baking at 350°C, leakage current analysis showed best fits for Poole-Frenkel conduction with a low activation energy of 0.57 eV. Baking the films resulted in adequate DC performance for applications of upto 15 V. The benefits of low-temperature hydrothermal synthesis makes it an acceptable technology for decoupling and similar power supply filter capacitor applications, where the voltage requirements are low and leakage current requirements are not stringent.

Acknowledgments This work is supported by the National Science Foundation (NSF) through its Engineering Research Center (ERC) program in Electronic Packaging (EEC-9402723) at the Packaging Research Center, Georgia Institute of Technology.

References

1. R.R. Tummala, M. Swaminathan, *Introduction to system-on-package* (McGraw-Hill Professional, New York, 2008), p. 423
2. R. Ulrich and L. Schaper (eds), "Integrated Passive Component Technology", IEEE Press/Wiley, (2003).
3. H. Windlass, P. Markondeya Raj, D. Balaraman, S.K. Bhattacharya, R. Tummala, IEEE Trans Adv Packag **26**(1), 10–16 (2003)
4. J.T. Dawley, P.G. Clem, Appl. Phys. Lett. **81**(16), 3206–3028 (2002)
5. J.F. Ihlefeld, B. Laughlin, A.H. Lowery, W. Borland, A. Kingon, J.P. Maria, J Electroceram **14**, 95–102 (2005)
6. R. Bacsa, P. Ravindranathan, J.P. Dougherty, J Mater Res **7**(2), 423–428 (1992)
7. E.B. Slamovich, I.A. Aksay, J Am Ceram. Soc. **79**(1), 239–247 (1997)
8. J.O. Eckert, C.C. Hung-Bouston, B.L. Gersten, M.M. Lencka, R. E. Riman, J Am Ceram Soc **79**, 2929–2939 (1996)
9. T. Noma, S. Wada, M. Yanu, T. Suzuki, J Appl Phys **80**(9), 5223–5233 (1996)
10. M.A. McCormick, E.B. Slamovich, J Eur Ceram Soc **23**, 2143–2152 (2003)
11. A.T. Chien, X. Xu, J.H. Kim, J. Sachleben, J.S. Speck, F.F. Lange, J Mater Res **14**(8), 3330–3339 (1999)
12. R. Kota, B.I. Lee, J Mater Sci Mater Electron **18**(12), 1221–1227 (2007)
13. D. Balaraman, P.M. Raj, L. Wan, I.R. Abothu, S. Bhattacharya, S. Dalmia, M.J. Lance, M. Swaminathan, M.D. Sacks, R.R. Tummala, J. Electroceram. **13**(1–3), 95–100 (2004)
14. P.M. Raj, B. Lee, D. Balaraman, N. Kang, M.J. Lance, H. Meyer, R. Tummala, J Am Ceram. Soc. **93**(9), 2764–2770 (2010)
15. A. Rose, Phys Rev **97**(6), 1538 (1955)
16. M. Amin, A. El-Shekeil, M. Mounir, M. Abu Elez, Die Angew Makromol Chem **193**, 13–20 (1991)
17. C.K. Tan, G.K.L. Goh, W.L. Cheah, Thin Solid Films **515**(16), 6577–6581 (2007)
18. W. Pennebaker, IBM J. Res. Dev. 687–697 (1969).
19. S. Zafar, R.E. Jones, B. Jiang, B. White, V. Kaushik, S. Gillespie, App Phys Lett **73**(24), 3533–3535 (1998)
20. M.C. Kao, S.Y. Lee, H.Z. Chen, S.L. Young, Thin Solid Films **516**, 8441–8446 (2008)
21. N. Konofaos, Z. Wang, S.N. Georga, C.A. Krontiras, M.N. Pisanias, J. Sotripoulus, E.K. Evangelou, J Elec Mater **34**(9), 1259–1263 (2005)